energies

Article

Analytical Model for the Pressure Performance Analysis of Multi-Fractured Horizontal Wells in Volcanic Reservoirs

Junqiang Wang [1], Xiaolong Qiang [2], Zhengcheng Ren [2], Hongbo Wang [2], Yongbo Wang [2] and Shuoliang Wang [3,*]

1 Jinan Bestune Times Power Technology Co., Ltd., Jinan 250000, China
2 The Second Gas Production Plant of PetroChina Changqing Oilfield Company, Yulin 719000, China
3 School of Energy, Faculty of Engineering, China University of Geosciences, Beijing 100083, China
* Correspondence: wangshuoliang@cugb.edu.cn

Abstract: Multi-fractured horizontal well (MFHW) technology is a key technology for developing unconventional reservoirs, which can generate a complex fracture network called a stimulated reservoir volume (SRV). Currently, there are many relative analytical models to describe the fluid seepage law, which are not suitable for volcanic reservoirs as of yet. The reasons are as follows: (1) due to the development of natural fractures, multi-scaled flow (matrix, natural fractures, SRV) should be considered to characterize MFHW flow in volcanic reservoirs; (2) non-Darcy flow and stress sensitivity should be considered simultaneously for seepage in volcanic reservoirs. Thus, this paper presents a novel MFHW analysis model of volcanic reservoirs that uses a multi-scale dual-porosity medium model and complex flow mechanisms. Laplace transformation, the Duhamel principle, the perturbation method and Stehfest numerical inversion are employed to solve the model to obtain dynamic pressure response curves. The results show that the pressure response curve can be divided into eight stages. Sensitivity analysis shows that the parameters of hydraulic fractures mainly affect the early flow stage. The parameters of the SRV region mainly affect the middle flow stage. The parameters of unreconstructed regions, non-Darcy flow and stress sensitivity mainly affect the late flow stage.

Keywords: volcanic reservoir; multi-fractured horizontal well; multi-scale flow; threshold pressure gradient; pressure transient analysis; stress sensitivity

Citation: Wang, J.; Qiang, X.; Ren, Z.; Wang, H.; Wang, Y.; Wang, S. Analytical Model for the Pressure Performance Analysis of Multi-Fractured Horizontal Wells in Volcanic Reservoirs. *Energies* **2023**, *16*, 879. https://doi.org/10.3390/en16020879

Academic Editor: Carlo Roselli

Received: 6 December 2022
Revised: 5 January 2023
Accepted: 9 January 2023
Published: 12 January 2023

1. Introduction

At present, the exploitation and development of conventional sandstone reservoirs have entered the middle and late stages. Unconventional oil and gas reservoirs account for an increasing proportion of the energy structure in China, especially volcanic reservoirs, which have attracted more and more attention. The reservoir spaces of volcanic reservoirs are diverse [1,2], including primary or dissolved pores and fractures [3]. Fractures, the main flow channel, are widely developed. Therefore, volcanic reservoirs have distinct characteristics of reservoirs and seepage. Considering the relative development of natural fractures in volcanic reservoirs, it is of great significance to propose a model that conforms to the production performance of volcanic reservoirs for the efficient development of volcanic reservoirs.

Multi-fractured horizontal wells are a vital technique for the development of volcanic oil reservoirs with natural fractures. Volume fracturing practices and micro-seismic monitoring technology indicate that a complex fracture network is formed by volume fracturing, which is essentially different from symmetrical fractures formed by conventional fracturing [4–6]. The principle of generating a complex network is that the vertical fractures with high conductivity near the horizontal well produced by multiple fractures coupled with surrounding natural fractures form a complex fracture network called the SRV (stimulated reservoir volume), achieving a three-dimensional reconstruction of the reservoir [7,8]. The

SRV refers to that in the process of hydraulic fracturing, the interlaced fracture network of natural fractures and artificial fractures increases the reconstruction volume and improves the initial production and final oil rate. The seepage model is the theoretical basis for well test analysis and production prediction, based on recognizing that volume fracturing can form complex fracture networks. Many domestic and foreign scholars have conducted a lot of research, where the most typical model of the analytical model is the linear flow model. Lee and Brockenbrough [9] first proposed the trilinear flow model and applied it to vertical fracture wells. Ozkan [10] introduced the trilinear flow model to fractured horizontal wells. Stalgorova [11] established a three-region model that contains the artificial fracture area, SRV area and USRV (unstimulated reservoir volume) area, but ignored the impact of the USRV area on horizontal well productivity. Then, Stalgorova [12] established a five-region model and verified it by comparing it with commercial software (Eclispse) results. Su Yuliang [13] established a four-region model of a fractured horizontal well by taking the threshold pressure gradient into account and analyzed the production model. Sureshjani [14] improved the five-region model. Foad Haeri [15] established a five-region linear model and carried out a sensitivity analysis. Jinghao Ji [16] established an improved five-region model for a multi-fractured horizontal well of a tight oil reservoir, which divided the USRV areas into complete and partial transformation areas, and carried out a sensitivity analysis. Based on the above linear flow model, some scholars improved it by considering certain parameters or integrating certain methods [17–24]. In addition, in recent years, many scholars have used the point source function and Laplace transformation to establish seepage models [25–28] of volume-fractured horizontal wells.

In summary, there are currently many relative analytical models to describe the fluid seepage law, which are not yet suitable for volcanic reservoirs. The reason is the description of seepage should consider both natural fractures and artificial fractures [29–36]. However, some of the above models consider the dual-porosity medium model [37–42], which has a constant scale and leads to an inaccurate description of fluid flow because it ignores the fluid flow in natural fractures of original reservoirs and simplifies natural fractures to single-porosity media.

The purpose of our work is to create a novel analytical model, which can accurately describe the flow characteristics of MFHWs in volcanic reservoirs. Unlike other unconventional reservoirs, volcanic reservoirs highly develop natural fractures, so the original reservoirs cannot be simply considered as having storage characteristics, and natural fractures also provide certain fluid flow characteristics. Therefore, when MFHW is used to develop volcanic reservoirs, the flow description is more complex than other unconventional reservoirs, and multi-scaled flow and multiple flow mechanisms should be considered. The novelty of the proposed model is as follows: (1) due to the development of natural fractures, multi-scaled flow (matrix, natural fractures, SRV) should be considered to characterize MFHW flow in volcanic reservoirs; (2) non-Darcy flow and stress sensitivity should be considered simultaneously for seepage in volcanic reservoirs. Therefore, this paper presents a novel MFHW analysis model of volcanic reservoirs, which uses a multi-scaled dual-porosity medium model and complex flow mechanisms. Laplace transformation, the Duhamel principle and the perturbation method are employed to solve the model. Then, the dynamic response curve of the corresponding pressure is obtained through Stehfest numerical inversion, and the sensitivity analysis of the parameters is carried out.

2. Materials and Methods

2.1. Physical Models and Assumptions

As can be seen in Figure 1, there is a multi-fractured horizontal well in the center of the volcanic reservoir with natural fractures. Based on the symmetry of the flow pattern of the wellbore, only one quarter of one fracture stage is enough to derive flow equations, as shown in Figure 2. The parameters are shown in Table 1.

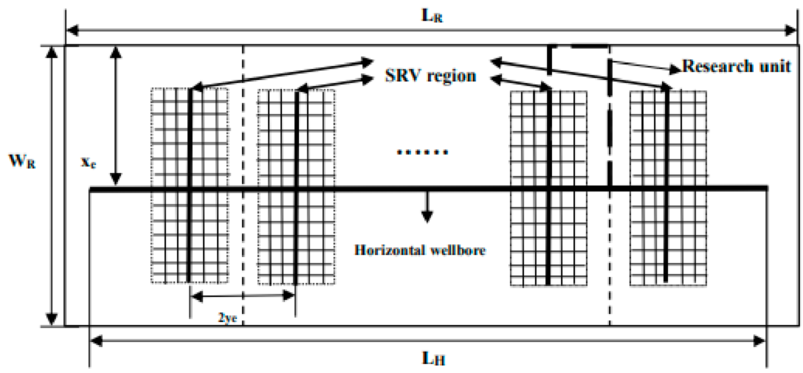

Figure 1. Schematic of a multi-fractured horizontal well in a volcanic oil reservoir.

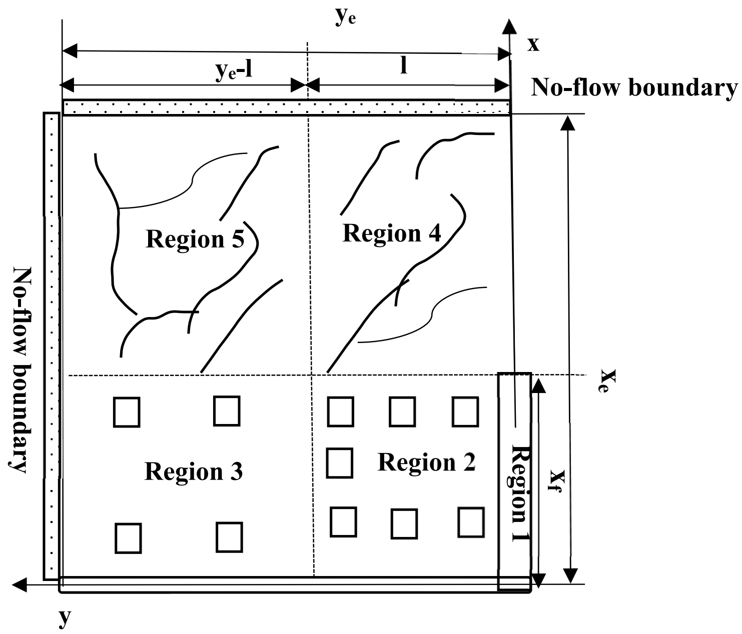

Figure 2. Schematic of the five-region flow model for a multi-fractured horizontal well.

Table 1. Symbol description.

Parameter	Symbol, Unit	Parameter	Symbol, Unit
Reservoir length	L_R, m	Reservoir width	W_R, m
Horizontal well length	L_H, m	Initial reservoir pressure	p_{ij}, Mpa
Permeability	k_{ij}, μm^2	Porosity	φ_{ij}, dimensionless
Elastic storativity ratio	ω, dimensionless	Inter-porosity flow coefficient	λi, dimensionless
Seepage velocity	V, m/h	Total compressibility coefficient	C_{tj}, MPa^{-1}
Single-fracture productionrate	q_F, m^3/d	Pressure conductivity coefficient	η, $\mu m^2/(mPa \cdot s \cdot MPa^{-1})$
Fracture interval	2ye, m	HF half-length	x_f, m
Viscosity	μ, mPa·s	FSRV half-length	l, m
Formation thickness	h, m	Oil volume factor	B, dimensionless
Threshold pressure gradient	λ_m, MPa/m	Permeability modulus	γ, MPa^{-1}
Initial permeability	$k_{i(fi)}$, μm^2	Bottom hole pressure	p_{wf}, Mpa
HF half-width	w, m		
Superscript of Laplace domain —/′			
Subscript of Dimensionless D			
Matrix or fracture system j = m, f			
Region No. I = 1~5			

As shown in Figure 2, the reservoir flow model is based on the Warren–Root model. The multi-fractured well in the volcanic reservoir is divided into five regions: Region 1 is the HF (hydraulic fracture) region, which is treated as a finite-conductivity fracture described by the single-porosity media model. Region 2 is the FSRV (fully stimulated reservoir volume) region. Region 3 is the PSRV (partly stimulated reservoir volume) region. Region 4 and region 5 are the USRV (unstimulated reservoir volume) regions. The SRV regions (regions 2 and 3) and the USRV regions (regions 4 and 5) can be treated as the dual-porosity media model, where the pores and fractures are the reservoir storage space, and the fractures are the flow channels.

This section is divided into seven subheadings. It provides a concise and precise description of the experimental results, their interpretation and the experimental conclusions that can be drawn.

In all of the regions, fracture permeability decreases as the formation pressure depletes. To account for the stress sensitivity, a stress-dependent permeability is adopted, following Kikani and Pedrosa [43]; the permeability modulus γ, which is used to describe stress sensitivity, is defined as

$$\gamma = \frac{1}{k}\frac{dk}{dp} \tag{1}$$

In the USRV regions, the formation has a tiny pore throat with ultra-low permeability, where non-Darcy flow is caused by the threshold pressure gradient. Therefore, the pseudo-TPG (threshold pressure gradient) approach is selected to describe the non-Darcy flow in this paper, expressed by the following equation [44]:

$$v = \begin{cases} -\dfrac{3.6k}{\mu}(grad(p) - \lambda_m) & grad(p) > \lambda_m \\ 0 & grad(p) < \lambda_m \end{cases} \tag{2}$$

The assumptions of the model are as follows:

1. According to the experimental results of volcanic reservoirs in Xinjiang, the outer boundary of the reservoir is enclosed. The reservoir thickness is h, the initial reservoir pressure is pi, the multi-fractured horizontal well is in the center of the reservoir and the working system of the well consists of constant production.
2. The hydraulic fractures are evenly spaced with the same properties. The height of the main fracture is equal to the thickness of the reservoir. The region between the two adjacent hydraulic fractures is impermeable.
3. There is isothermal flow of a single-phase micro-compressible liquid, which neglects the gravity, capillary force and resistance in the wellbore.
4. The liquid flows through the SRV region, the hydraulic fracture and horizontal wells in sequence.
5. The permeability stress sensitivity cannot be neglected in all of the regions; the threshold pressure gradient cannot be neglected in the USRV regions.

2.2. Mathematical Model and Solution

2.2.1. Dimensionless Parameters

On the basis of the physical model and assumptions, we establish the mathematical models of different regions. To facilitate the derivation, we define the following dimensionless variables (Table 2). The subscript i = 1–5 represents the five regions, and j = f or m represents the fracture system or the matrix system.

Table 2. Dimensionless parameters.

Dimensionless Parameter	Formula
Dimensionless pressure	$p_{ijD} = \dfrac{k_{2fi}h(p_i - p_{ij})}{1.842 \times 10^{-3} q_F \mu B}$
Dimensionless production rate of single HF	$q_{FD} = \dfrac{1.842 \times 10^{-3} q_F \mu B}{k_{2f}h\left(p_i - p_{wf}\right)}$
Dimensionless time	$t_D = \dfrac{3.6k_{2fi}t}{\mu(\phi c_t)_{2(f+m)}x_f^2}$
Dimensionless length	$x_D = \dfrac{x}{x_f}, y_D = \dfrac{y}{x_f}, x_{eD} = \dfrac{x_e}{x_f}, y_{eD} = \dfrac{y_e}{x_f}$
Dimensionless HF half-width	$w_D = \dfrac{w}{x_f}$
Dimensionless SRV area width	$l_D = \dfrac{l}{x_f}$
Dimensionless conductivity coefficient	$\eta_{iD} = \dfrac{\eta_i}{\eta_2}$
Inter-porosity flow coefficient	$\lambda_i = \alpha \dfrac{k_{im}}{k_{ifi}} x_f^2$
Elastic storativity ratio	$\omega_i = \dfrac{(C_t\phi)_{if}}{(C_t\phi)_{if} + (C_t\phi)_{im}}$
Dimensionless hydraulic fracture conductivity	$C_{FD} = \dfrac{k_{1fi}w}{k_{2fi}x_f}$
Mobility ratio	$M_{32} == \dfrac{k_{2fi}/\mu}{k_{3fi}/\mu}$
Dimensionless TPG	$\lambda_D = C_L \lambda_m x_f$
Dimensionless permeability modulus	$\gamma_D = \dfrac{1.842 \times 10^{-3} q_F \mu B}{k_{2fi}h}\gamma$
Intermediate variable in region 4 and region 5	$T = \dfrac{k_{4,5fi}hx_F\lambda_m}{1.842 \times 10^{-3} q_F \mu B}$
Intermediate variable in region 2 and region 3	$G = \dfrac{k_{2fi}hx_F\lambda_m}{1.842 \times 10^{-3} q_F \mu B}$

2.2.2. Mathematical Model of Regions 4 and 5

In regions 4 and 5, it is assumed that there is only a one-dimensional linear flow in the x-direction; additionally, the threshold pressure gradient (TPG) is used to describe non-Darcy flow according to Equation (1), which can be expressed as

$$v = -\frac{3.6k_{if}}{\mu}\left(grad\left(p_{if}\right) - \lambda_m\right) \tag{3}$$

When the formation pressure decreases in the production process, the permeability stress sensitivity cannot be neglected, according to the definition of the permeability modulus in Equation (1), which can be expressed as

$$k = k_i e^{-\gamma(p_i - p)} \tag{4}$$

where p_i is the initial formation pressure, and k_i is the permeability at the initial condition.

Therefore, as shown in Figure 2, the outer boundary of region 5 is impermeable and its inner boundary is the outer boundary of region 3. Hence, combining the initial conditions and boundary conditions, we can obtain the dimensionless mathematical model of region 5:

$$\begin{cases} e^{-\gamma_D p_{5fD}}\left[\dfrac{\partial^2 p_{5fD}}{\partial {x_D}^2} + (T\gamma_D - \lambda_{mD})\dfrac{\partial p_{5fD}}{\partial x_D}\right] + \lambda_5(p_{5mD} - p_{5fD}) = \dfrac{\omega_5}{\eta_{5D}}\dfrac{\partial p_{5fD}}{\partial t_D} \\ \dfrac{1-\omega_5}{\eta_{5D}}\dfrac{\partial p_{5mD}}{\partial t_D} + \lambda_5(p_{5mD} - p_{5fD}) = 0 \\ \left.\dfrac{\partial p_{5fD}}{\partial x_D}\right|_{x_D = x_{eD}} = 0 \\ p_{5fD}\Big|_{x_D=1} = p_{3fD}\Big|_{x_D=1} \end{cases} \tag{5}$$

Because regions 4 and 5 are both USRV regions and have the same properties, by using the same method as region 5, the dimensionless mathematical model of region 4 can be obtained:

$$\begin{cases} e^{-\gamma_D p_{4fD}}\left[\dfrac{\partial^2 p_{4fD}}{\partial {x_D}^2} + (T\gamma_D - \lambda_{mD})\dfrac{\partial p_{4fD}}{\partial x_D}\right] + \lambda_4(p_{4mD} - p_{4fD}) = \dfrac{\omega_4}{\eta_{4D}}\dfrac{\partial p_{4fD}}{\partial t_D} \\ \dfrac{1-\omega_4}{\eta_{4D}}\dfrac{\partial p_{4mD}}{\partial t_D} + \lambda_4(p_{4mD} - p_{4fD}) = 0 \\ \left.\dfrac{\partial p_{4fD}}{\partial x_D}\right|_{x_D = x_{eD}} = 0 \\ p_{4fD}\Big|_{x_D=1} = p_{2fD x_D=1} \end{cases} \tag{6}$$

2.2.3. Mathematical Model of Region 3

With the assumption of a linear flow in the y-direction, and taking the stress sensitivity into consideration, which is described by Equation (4), in PSRV region 3, the oil flow follows Darcy's law. Combining the initial conditions and boundary conditions, and considering the fluid flowing from region 5 into region 3, the dimensionless model is as follows:

$$\begin{cases} e^{-\gamma_D p_{3fD}}\dfrac{\partial^2 p_{3fD}}{\partial {y_D}^2} + \dfrac{k_{5fi}}{k_{3fi}} e^{-\gamma_D p_{5fD}}\left.\left(\dfrac{\partial p_{5fD}}{\partial x_D} + G\right)\right|_{x_D=1} + \lambda_3(p_{3mD} - p_{3fD}) = \dfrac{\omega_3}{\eta_{3D}}\dfrac{\partial p_{3fD}}{\partial t_D} \\ \dfrac{1-\omega_3}{\eta_{3D}}\dfrac{\partial p_{3mD}}{\partial t_D} + \lambda_3(p_{3mD} - p_{3fD}) = 0 \\ \left.\dfrac{\partial p_{3fD}}{\partial y_D}\right|_{y_D = y_{eD}} = 0 \\ p_{3fD}\Big|_{y_D=l_d} = p_{2fD}\Big|_{y_D=l_d} \end{cases} \tag{7}$$

2.2.4. Mathematical Model of Region 2

With the assumption of a linear flow in the y-direction, and following a similar derivation process to region 3, the dimensionless seepage model to describe the oil flow in region 2 is given by

$$\begin{cases} e^{-\gamma_D p_{2fD}} \dfrac{\partial^2 p_{2fD}}{\partial {y_D}^2} + \dfrac{k_{4fi}}{k_{2fi}} e^{-\gamma_D p_{4fD}} \left(\dfrac{\partial p_{4fD}}{\partial x_D} + G \right) \Big|_{x_D=1} + \lambda_2 (p_{2mD} - p_{2fD}) = \dfrac{\omega_2}{\eta_{2D}} \dfrac{\partial p_{2fD}}{\partial t_D} \\ \dfrac{1-\omega_2}{\eta_{2D}} \dfrac{\partial p_{2mD}}{\partial t_D} + \lambda_3 (p_{2mD} - p_{2fD}) = 0 \\ e^{-\gamma_D p_{2fD}} \dfrac{\partial p_{2fD}}{\partial y_D} \Big|_{y_D=l_D} = \dfrac{1}{M_{32}} e^{-\gamma_D p_{3fD}} \dfrac{\partial p_{3fD}}{\partial y_D} \Big|_{y_D=l_D} \\ p_{2fD} \Big|_{y_D=w_D/2} = p_{1fD} \Big|_{y_D=w_D/2} \end{cases} \tag{8}$$

2.2.5. Mathematical Model of Region 1

The flow in the HF region is also assumed to be a linear flow in the x-direction. Taking into account the effect of stress sensitivity, the governing equation for the flow in HF can be obtained as follows:

$$\begin{cases} e^{-\gamma_D p_{1fD}} \dfrac{\partial^2 p_{1fD}}{\partial {x_D}^2} + \dfrac{2}{C_{FD}} e^{-\gamma_D p_{2fD}} \dfrac{\partial p_{2fD}}{\partial y_D} \Big|_{y_D=w_D/2} = \dfrac{1}{\eta_{1D}} \dfrac{\partial p_{1fD}}{\partial t_D} \\ e^{-\gamma_D p_{1fD}} \dfrac{\partial p_{1fD}}{\partial x_D} \Big|_{x_D=0} = -\dfrac{\pi}{C_{FD}} \\ \dfrac{\partial p_{1fD}}{\partial x_D} \Big|_{x_D=1} = 0 \end{cases} \tag{9}$$

2.2.6. Solution of Model

It can be seen from Equations (5)–(9), that the dimensionless seepage model in regions 1–5 has a strong nonlinearity, meaning the solution cannot be solved directly. Through the Pedrosa transformation [45], the nonlinearity of the equation is eliminated:

$$p_{jD} = -\frac{1}{\gamma_D} \ln(1 - \gamma_D \xi_{jD}), j = 1,2,3,4,5 \tag{10}$$

Additionally, the following perturbation transformation formula is introduced:

$$\xi_{jD} = \xi_{jD0} + \gamma_D \xi_{jD1} + {\gamma_D}^2 \xi_{jD2} + \ldots j = 1,2,3,4,5 \tag{11}$$

$$\frac{1}{1 - \gamma_D \xi_{jD}} = 1 + \gamma_D \xi_{jD} + {\gamma_D}^2 {\xi_{jD}}^2 + \ldots j = 1,2,3,4,5 \tag{12}$$

$$-\frac{1}{\gamma_D} \ln(1 - \gamma_D \xi_{jD}) = \gamma_D \xi_{jD} + \frac{1}{2} \gamma_D {\xi_{jD}}^2 + \ldots j = 1,2,3,4,5 \tag{13}$$

Considering that the actual dimensionless permeability modulus is a small amount, the zeroth-order perturbation solution can satisfy the requirement of precision. Therefore, the seepage model in each region is handled by adopting the Pedrosa method under the zeroth-order perturbation solution before being applied to the Laplace transformation. Finally, the solution of the dimensionless bottom hole pressure in the Laplace space is obtained, the derivation process can refer to in Appendix A.

$$\overline{p}_{wD0} = {\xi'}_{3D0}(x_D = 0) = \frac{\pi}{C_{FD} s \sqrt{c_3} \tanh(\sqrt{c_3})} + \frac{2B}{C_{FD}} \left(\frac{k_{4fi}}{k_{2fi} c_2} - \frac{k_{5fi}}{k_{3fi} c_1} \right) \frac{G}{s c_3} + \frac{2A}{C_{FD}} \frac{k_{4fi}}{k_{2fi} c_2} \frac{G}{s c_3} \tag{14}$$

where

$$c_3 = \frac{2A}{C_{FD}} + \frac{s}{\eta_{1D}}$$

$$A = \frac{-\left[\sqrt{c_2}\sinh\left(\sqrt{c_2}\left(\frac{w_D}{2} - l_D\right)\right) + c_0\sqrt{c_2}\cosh\left(\sqrt{c_2}\left(\frac{w_D}{2} - l_D\right)\right)\right]}{\cosh\left(\sqrt{c_2}\left(\frac{w_D}{2} - l_D\right)\right) + c_0\sinh\left(\sqrt{c_2}\left(\frac{w_D}{2} - l_D\right)\right)}$$

$$B = \frac{c_0\sqrt{c_2}}{\cosh\left(\sqrt{c_2}\left(\frac{w_D}{2} - l_D\right)\right) + c_0\sinh\left(\left(\sqrt{c_2}\left(\frac{w_D}{2} - l_D\right)\right)\right)}$$

$$c_0 = \frac{\sqrt{c_1}\tanh(\sqrt{c_1}(l_D - y_{eD}))}{M_{32}\sqrt{c_2}}$$

$$c_2 = \frac{k_{4fi}}{k_{2fi}}\beta_2 + f_{s2}$$

$$c_1 = \frac{k_{5fi}}{k_{3fi}}\beta_1 + f_{s3}$$

$$\beta_2 = \frac{m_2 e^{m_1(1-x_{eD})} - m_2 e^{m_2(1-x_{eD})}}{\left(-\frac{m_2}{m_1}\right)e^{m_1(1-x_{eD})} + e^{m_2(1-x_{eD})}}$$

$$\beta_1 = \frac{r_2 e^{r_1(1-x_{eD})} - r_2 e^{r_2(1-x_{eD})}}{\left(-\frac{r_2}{r_1}\right)e^{r_1(1-x_{eD})} + e^{r_2(1-x_{eD})}}$$

$$m_1 = \frac{\lambda_D + \sqrt{\lambda_D{}^2 + 4f_{s4}}}{2}$$

$$m_2 = \frac{\lambda_D - \sqrt{\lambda_D{}^2 + 4f_{s4}}}{2}$$

$$r_1 = \frac{\lambda_D + \sqrt{\lambda_D{}^2 + 4f_{s5}}}{2}$$

$$r_2 = \frac{\lambda_D - \sqrt{\lambda_D{}^2 + 4f_{s5}}}{2}$$

$$f_{si} = \frac{\lambda_i(1-\omega_i)s}{\lambda_i\eta_{iD} + (1-\omega_i)s} + \frac{\omega_i s}{\eta_{iD}} i = 2,3,4,5$$

$$M_{32} = \frac{k_{2fi}/\mu}{k_{3fi}/\mu}$$

Taking the skin factor and wellbore storage effects into consideration, the dimensionless wellbore storage coefficient C_D and the skin coefficient S are introduced with the help of the Duhamel principle in the Laplace space. The bottom hole pressure is

$$\overline{p}_{wD}(C_D, S) == \frac{s\overline{p}_{wD0} + S}{s[1 + C_D s(s\overline{p}_{wD0} + S)]} \tag{15}$$

According to the above formula, the bottom hole pressure is related to the TPG, stress sensitivity, hydraulic fracture parameters, SRV and USRV parameters, and sensitivity analysis is carried out for these parameters in the Results and Discussion section.

Applying Stehfest numerical inversion to Equation (15), the perturbation transformation is applied to solve the actual bottom hole pressure, which is as follows:

$$p_{wD} = -\frac{\ln\left[1 - \gamma_D L^{-1}(\overline{p}_{wD0})\right]}{\gamma_D} \tag{16}$$

In Equation (16), Stehfest numerical inversion is applied [46]:

$$V(i) = (-1)^{N/2+i} \sum_{k=(i+1)/2}^{\min(i,N/2)} \frac{k^{N/2}(2k)!}{(N/2-k)!k!(k-1)!(i-k)!(2k-i)!} \tag{17}$$

$$f(t) = \frac{\ln(2)}{t} \sum_{i=1}^{N} V(i)\widetilde{f}(s_i) \tag{18}$$

$$s_i = i\frac{\ln(2)}{t} \tag{19}$$

2.2.7. Multi-Fracture Superposition Processing

As shown in Figure 3, we consider the bottom hole pressure to vary for different fractures in constant production. According to the shape parameters of the fracture (the ratio of the transverse control length to the vertical control length), the fracture can be divided into two parts: the internal and the end [47].

$$\text{Internal fracture}: \delta_{in} = \frac{W_R}{L_H/(N-1)} \tag{20}$$

$$\text{End fracture}: \delta_{out} = \frac{W_R}{L_R - L_H} \tag{21}$$

Suppose that the number of fractures is N, and the dimensionless pressure and production expression of multi-fractured wells with a uniform distribution of hydraulic fractures is

$$\text{Constant production working system}: p_{ND} = \frac{p_D(t_D,\delta_{in}) \cdot p_D(t_D,\delta_{out})}{p_D(t_D,\delta_{in}) + (N-1)p_D(t_D,\delta_{out})} \tag{22}$$

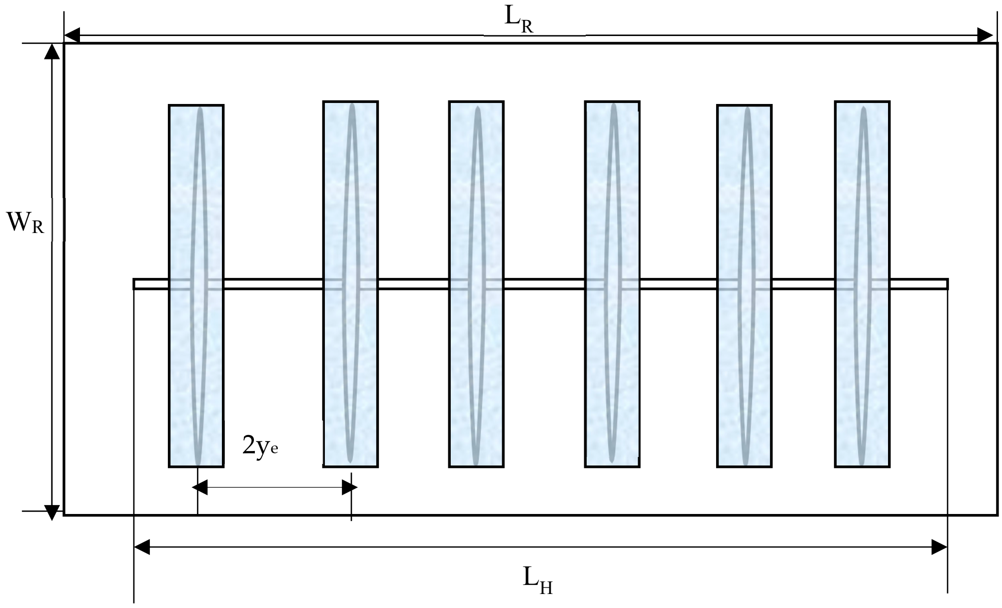

Figure 3. Different fracture arrangement of multi-fractured horizontal well.

3. Results and Discussion

The reservoir parameters and MFHW parameters of the model are collected from the volcanic reservoir in Xinjiang, Southwest China. The length, width and height of the reservoir are 1800 m, 600 m and 15 m, respectively. The length of the horizontal well is 1400 m. There are eight hydraulic fractures, whose half-length and half-width are 100 m and 20 m. The porosity, permeability and half-width of the hydraulic fracture are 0.25, 20,000 mD and 0.01 m, respectively. The porosity and permeability of the fractures in regions 2–5 are 0.06, 0.06, 0.02 and 0.02, and 1000 mD, 100 mD, 10 mD and 10 mD, respectively. The porosity and permeability of the matrix in regions 2–5 are 0.14, 0.14, 0.2 and 0.2, and 0.108 mD, 0.108 mD, 0.108 mD and 0.108 mD, respectively. The rock compressibility is 0.00023 MPa^{-1}. The fluid compressibility is 0.0005 MPa^{-1}. The oil viscosity is 1.02 mPa·s, the formation volume factor is 1.2 and the production of a single fracture is 16 m^3/d. TPG is 0.02 MPa/m, and the permeability modulus is 0.02 MPa^{-1}. Considering the skin factor and dimensionless wellbore storage coefficient, the pressure curve of the volcanic reservoir is calculated with the above model and parameters, as shown in Figure 4.

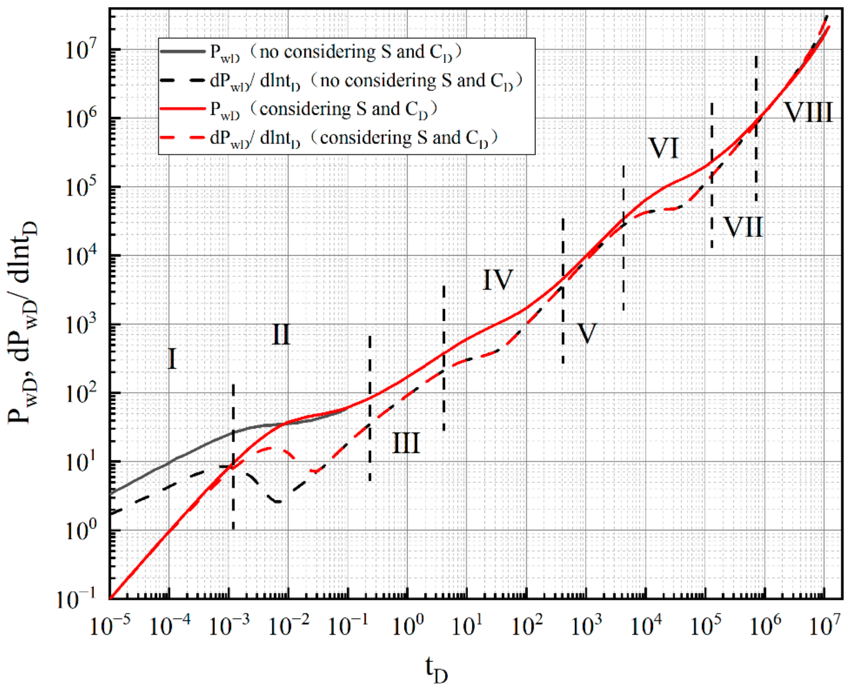

Figure 4. Pressure response of a multi-fractured horizontal well in a volcanic reservoir.

3.1. Dynamic Pressure Response Curve

As can be seen in Figure 4, the flow pattern can be divided into eight stages: (1) bi-linear flow in the HF and FSRV regions, where the pressure curve is parallel to the pressure derivative and the slope is 1/4, and when considering the skin factor and wellbore storage coefficient, the bi-linear flow is covered up; (2) inter-porosity flow between the fracture and matrix in the FSRV region, where a groove exists in the pressure derivative; (3) linear flow in the PSRV region, where the pressure curve is parallel to the pressure derivative and the slope is 1/4; (4) inter-porosity flow between the fracture and matrix in the PSRV region, where the derivative of the pressure gradient is slowed (approximate grooves); (5) linear flow in the USRV region; (6) inter-porosity flow between the fracture and matrix in the USRV region, where the derivative of the pressure gradient is slowed (approximate grooves); (7) complex linear flow in all of the regions (FSRV + PSRV + USRV); (8) boundary control flow.

3.2. Model Validation and Comparison

In the case of ignoring the wellbore storage effect and skin effect, the above parameters are still used, except l = ye and l = 0.2 ye. We obtain the corresponding pressure response curve, which is compared with the Ozkan model. As shown in Figure 5, the result of l = ye is completely coincidental with the Ozkan model, which verifies the model. As for the pressure response curve of l = 0.2 ye, the USVR area between the fractures could affect the flow pattern in the late period. Therefore, the dimensionless pressure is less than that of the Ozkan model.

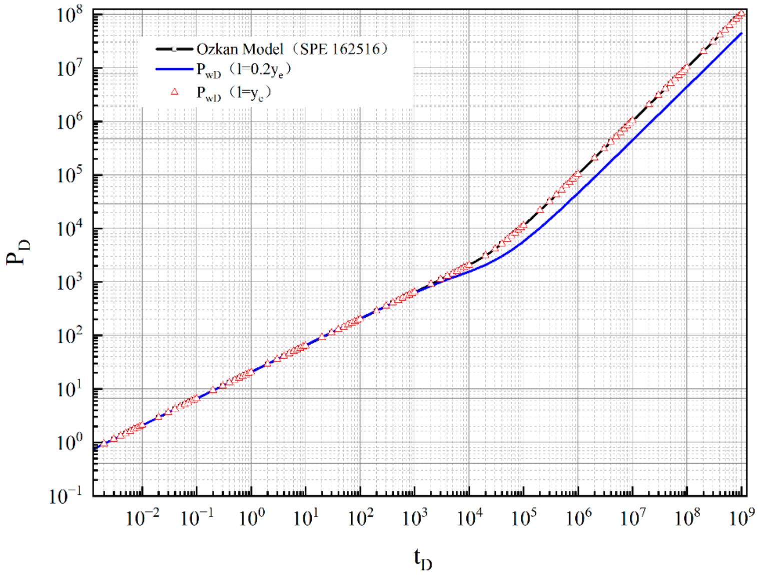

Figure 5. Model verification and comparison.

The dynamic response curves are calculated based on the field data of a fractured horizontal well in the Xinjiang Oilfield, which are compared with the actual well testing data. It can be seen from Figure 6 that the calculation results of the proposed model are in good agreement with the actual test results, and the flow characteristics of MFHWs in volcanic reservoirs are obvious.

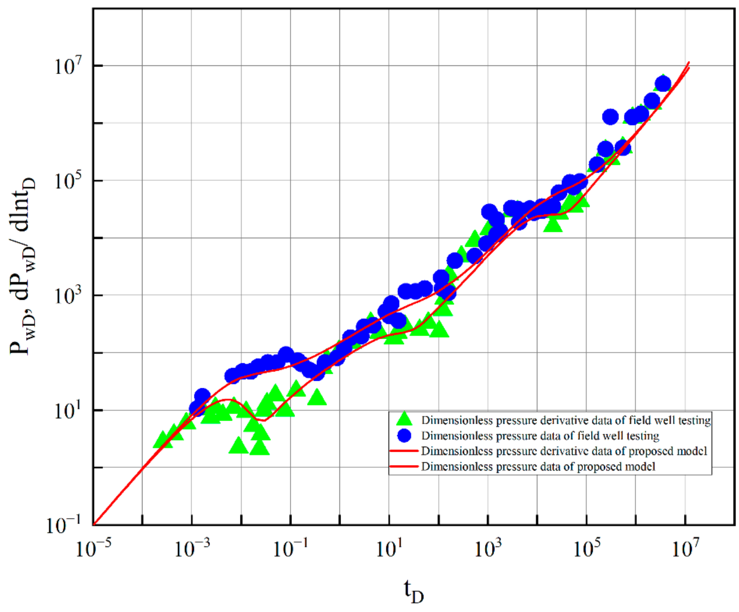

Figure 6. Model validation and comparison.

3.3. Sensitivity Analysis

3.3.1. Effect of TPG

Figure 7 shows the influence of TPG on the dynamic pressure, where it is found that TPG affects the flow in the middle and late stages, mainly affecting the flow in the later stage. When the starting pressure gradient is bigger, the later consumption is more obvious. The curves of the dimensionless pressure and pressure derivative cock earlier and higher.

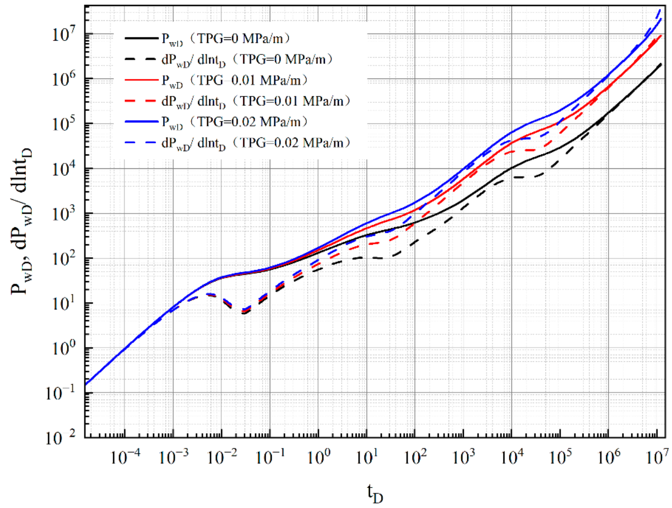

Figure 7. The effect of TPG on the pressure response.

3.3.2. Effect of Stress Sensitivity

Figure 8 shows that in the production process of MFHWs in volcanic reservoirs, the fracture permeability of each region changes with the decrease in the formation pressure. Different permeability moduli represent different stress-sensitive effects. From the pressure response curve, we can see that stress sensitivity affects the late flow stage and has little effect on the early and middle stages. This is because the pressure drop is smaller in the early stage, and the permeability varies slightly with the formation pressure. As time goes on, the permeability stress influence increases. The greater the permeability modulus, the more obvious the stress-sensitive phenomenon, which shows that more upward dimensionless pressure and pressure derivative curves are found in the later period.

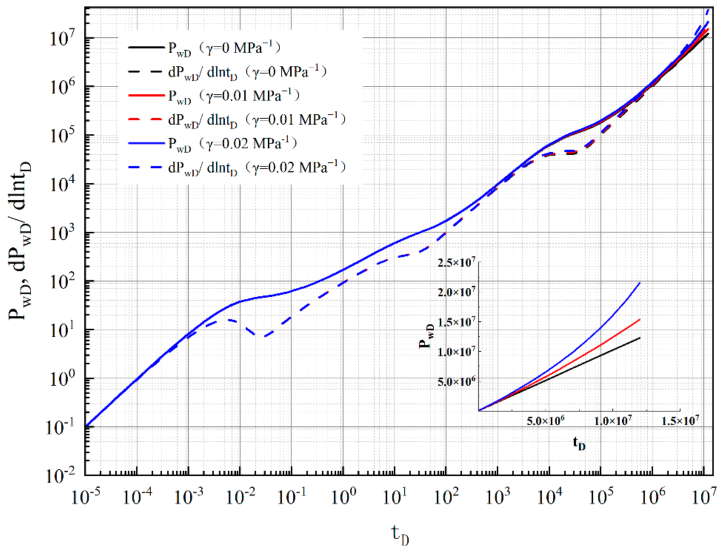

Figure 8. The effect of stress sensitivity on the pressure response.

3.3.3. Effect of Hydraulic Fracture Conductivity

Figure 9 shows the relationship between the hydraulic fracture conductivity and the response curve of pressure. Considering that the hydraulic fracture conductivity coefficient is 100 mD·m, 150 mD·m and 200 mD·m, other parameters remain unchanged. According to the pressure response curve, the hydraulic fracture conductivity coefficient affects the early flow stage, but the degree of influence is small. When the hydraulic fracture conductivity coefficient is greater, the longer the duration of the bi-linear flow, the less obvious the FSRV inter-porosity flow. It can be seen that the inter-porosity flow groove curve is narrower on the pressure derivative curve.

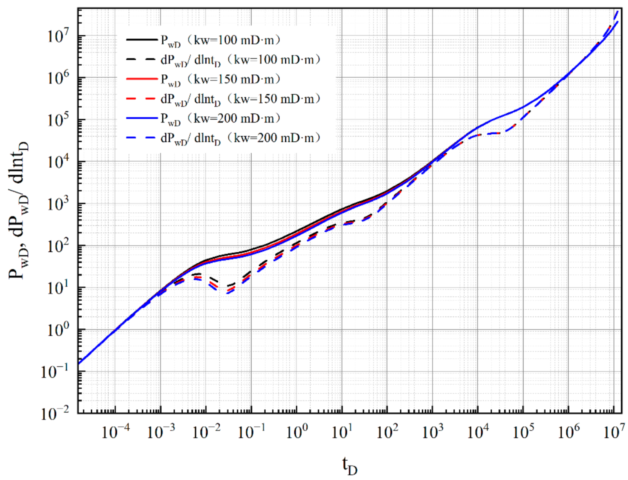

Figure 9. The effect of the hydraulic fracture conductivity coefficient on the pressure response.

3.3.4. Effect of FSRV Half-Length

Figure 10 shows the relationship between the length of the FSRV area and the pressure response curve. Considering that the half-length of the FSRV area is 100 m, 150 m and 200 m, the other parameters remain unchanged. Through comparative analysis, we can find that the length of the FSRV area has a greater influence in the middle and late stages of the flow. When the length of the hydraulic fracture becomes larger and larger, it is shown that the transverse-to-longitudinal ratio of the FSRV area is increased, and the longitudinal channeling is not obvious. At the same time, the late flow in the USRV area is easier to cover up. The pressure response curve shows that, with the increase in the half-length of the FSRV area, the pressure derivative groove is narrower and shallower, and the later inter-porosity flow is easier to cover up.

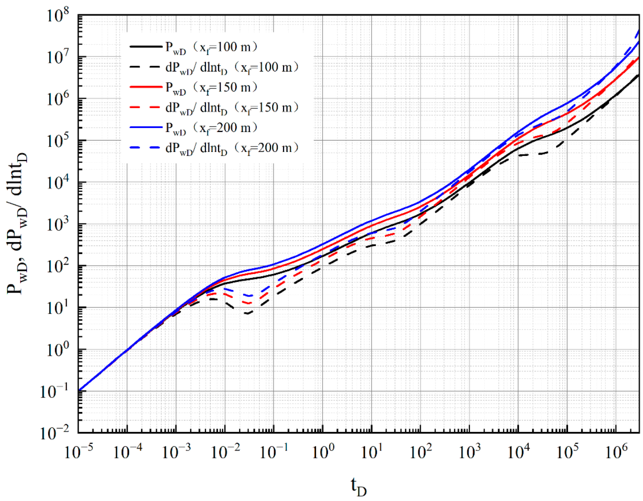

Figure 10. The effect of the FSRV half-length on the pressure response.

3.3.5. Effect of FSRV Half-Width

Figure 11 shows the relationship between the half-width of the FSRV area and the pressure response curve. When the half-width of the FSRV area is 20 m, 60 m and 100 m, the other parameters remain unchanged. It can be seen that the width of the FSRV area is mainly affected by the middle period of the flow stage, especially the inter-porosity flow and linear flow in the FSRV and PSRV areas. When the half-width of the FSRV area is larger, it shows that the larger the volume of the fracture network fracturing, the better the fracturing effect, and the smaller the PSRV area, which indicates that the inter-porosity flow in the FSRV area is more obvious, and the flow in the PSRV area is shorter. The pressure response curve is as follows: with the increase in the half-width, the volume of the FSRV area increases, and the inter-porosity flow is more obvious, which covers up the linear flow in the PSRV area. It is verified in the pressure response curve that the pressure derivative grooves appear wider and deeper.

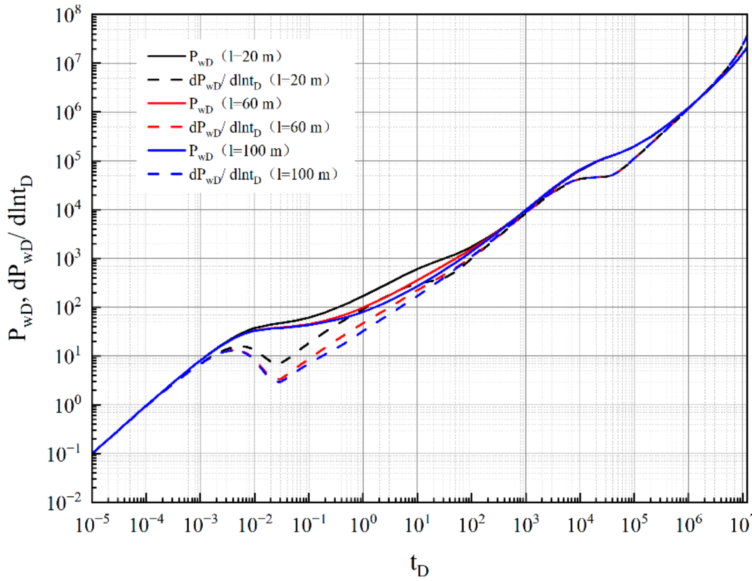

Figure 11. The effect of the FSRV half-width on the pressure response.

3.3.6. Effect of FSRV Inter-Porosity Flow Coefficient

Figure 12 shows the effect of the inter-porosity flow coefficient on the pressure performance of MFHWs in volcanic reservoirs. It shows that the inter-porosity flow coefficient has a significant effect on the early period and determines the position of the grooves on the pressure derivative curve. Assuming that the FSRV inter-porosity flow coefficient is 1.5, 15 and 150, when the inter-porosity flow coefficient is larger, this indicates that the inter-porosity flow resistance is small, and the inter-porosity flow groove position is closer to the right, which shows that the inter-porosity flow occurs earlier in the fracture system. The pressure response curve is as follows: with the increase in the flow coefficient in the FSRV area, the dimensionless pressure curve is lower in the FSRV area, and the inter-porosity flow grooves in the FSRV area appear earlier, wider and deeper on the dimensionless pressure derivative curve.

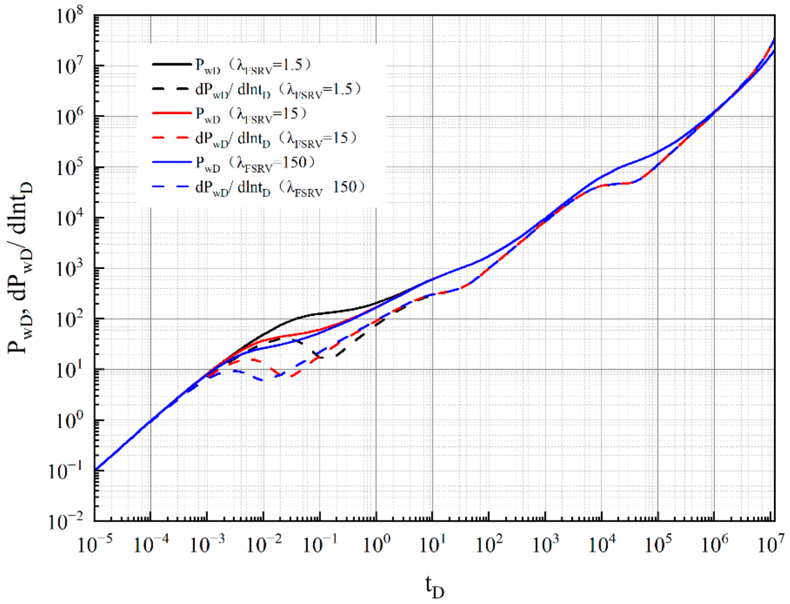

Figure 12. The effect of the FSRV inter-porosity flow coefficient on the pressure response.

3.3.7. Effect of FSRV Storativity Ratio

Figure 13 shows the relationship between the pressure response curve and the FSRV storativity ratio. According to the response curve, we know that the FSRV storativity ratio only affects the FSRV inter-porosity flow stage, and the effect is not very obvious. The storativity ratio affects the width and depth of the grooves in the FSRV area of the dimensionless pressure derivative curve. Considering that the FSRV storativity ratios are 0.008, 0.04 and 0.08, when the storativity ratio is smaller, there is less fluid storage, and the fracture system causes a great pressure drop in a short time; then, it takes a long time to make the matrix pressure and fracture pressure decreases synchronously, meaning the groove is wider and deeper.

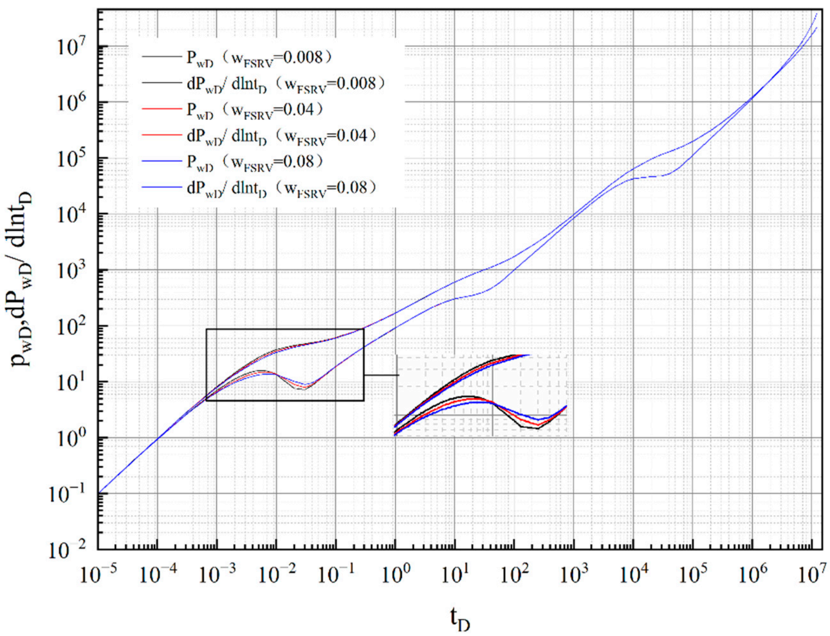

Figure 13. The effect of the FSRV storativity ratio on the pressure response.

3.3.8. Effect of FSRV Fracture Permeability

Figure 14 shows the relationship between the fracture permeability and the pressure response curve in the FSRV area. Considering that the fracture permeability of the FSRV area is 1000 mD, 3000 mD and 5000 mD, the other parameters remain unchanged. Through comparison and analysis, the FSRV fracture permeability mainly affects the early and middle flow stages, and the flow of the FSRV and USRV zones. The higher the FSRV fracture permeability, the smaller the flow resistance of the fracture system; the bi-linear flow stage is more obvious and the pressure drops faster, but the inter-porosity flow coefficient becomes smaller, which means that the later the inter-porosity flow occurs, the longer the duration of the early linear flow. As shown in the response curve, the lower the FSRV fracture permeability, the deeper and wider the groove in the pressure derivative, and the higher the position of the pressure curve.

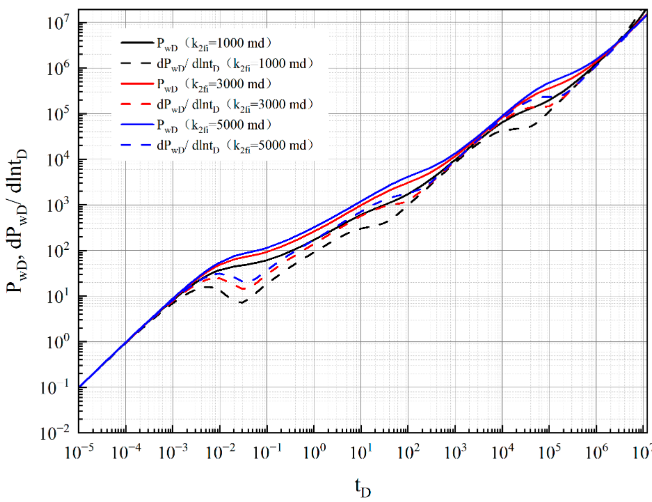

Figure 14. The effect of FSRV fracture permeability on the pressure response.

3.3.9. Effect of USRV Inter-Porosity Flow Coefficient

Figure 15 compares the difference in the pressure response curves with different inter-porosity coefficients in the USRV area, which represents the percolation law of a volcanic reservoir with dual-medium characteristics. When the inter-porosity coefficient is 0.0006, 0.06 and 1.2, the other parameters remain unchanged. The USRV inter-porosity coefficient controls the inter-porosity flow stage of the USRV area. When the coefficient is large, the pressure derivative curve shows that the position of the groove is low.

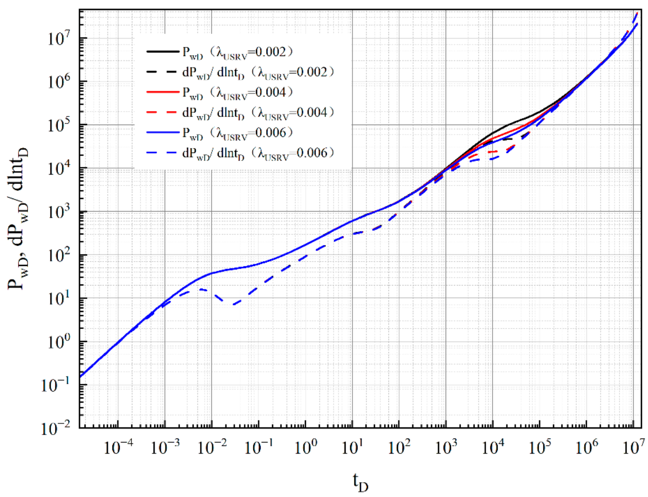

Figure 15. The effect of the USRV inter-porosity coefficient on the pressure response.

4. Conclusions

This paper presents an analytical model for the pressure analysis of MFHWs in volcanic reservoirs. The model is verified, and a field example is presented. The novelty of the proposed model is as follows: (1) due to the development of natural fractures, multi-scaled flow (matrix, natural fractures, SRV) should be considered to characterize the MFHW flow in volcanic reservoirs; (2) non-Darcy flow and stress sensitivity should be considered simultaneously for seepage in volcanic reservoirs. By investigating the transient pressure behavior and analyzing the effects of related influential parameters, the main conclusions of this paper are as follows:

1. This new analytical model for MFHWs in volcanic reservoirs, considering a multi-scaled flow and complex flow mechanisms (non-Darcy flow and stress sensitivity), is different from the previous models and conforms to the real situation, where the reservoir is subdivided into five continuous flow regions: USRV regions 4 and 5, FSRV region 2, PSRV region 3 and HF region 1, where the effects of both the non-Darcy flow and stress sensitivity are considered. Laplace transformation, the Duhamel principle and the perturbation method are employed to solve the model.
2. According to the field parameters, the pressure response curve can be obtained through the analytical model, which can be divided into eight stages, namely, bi-linear flow in the HF and FSRV regions, inter-porosity flow in the FSRV region, linear flow in the PSRV region, inter-porosity flow in the PSRV region, linear flow in the USRV region, inter-porosity flow in the USRV region, linear flow in all of the regions and boundary control flow.
3. Sensitivity analysis shows that the parameters of hydraulic fractures mainly affect the early flow stage. The parameters of the SRV region mainly affect the middle flow stage. The parameters of the USRV region, non-Darcy flow and stress sensitivity mainly affect the late flow stage. Furthermore, TPG, stress sensitivity and the mode of storage and seepage in the unstimulated reservoir volume region have a significant influence on the transient pressure performance and seepage law.

Author Contributions: Conceptualization, J.W. and Z.R.; methodology, J.W.; software, J.W.; validation, J.W. and H.W.; formal analysis, J.W.; investigation, Z.R.; resources, Y.W.; data curation, X.Q.; writing—original draft preparation, J.W.; writing—review and editing, S.W.; visualization, J.W. and H.W.; super-vision, S.W.; project administration, Y.W.; funding acquisition, J.W. All authors have read and agreed to the published version of the manuscript.

Funding: This research received no external funding.

Data Availability Statement: The data presented in this study are available on request from the corresponding author. The data are not publicly available because it is confidential.

Conflicts of Interest: The authors declare no conflict of interest.

Appendix A

According to Equations (10)–(13), through perturbation transformation and Laplace transformation, the seepage governing equations in Laplace space are obtained.

The seepage governing equation of region 5 is as follows:

$$\begin{cases} e\dfrac{\partial^2 \xi'_{5D0}}{\partial {x_D}^2} - \lambda_{mD}\dfrac{\partial \xi'_{5D0}}{\partial x_D} - f_{s5}\xi'_{5D0} = 0 \\ \left.\dfrac{\partial \xi'_{5D0}}{\partial x_D}\right|_{x_D = x_{eD}} = 0 \\ \xi'_{5D0}|_{x_D=1} = \xi'_{3D0}|_{x_D=1} \end{cases} \tag{A1}$$

The seepage governing equation of region 4 is as follows:

$$\begin{cases} e\dfrac{\partial^2 \xi'_{4D0}}{\partial x_D{}^2} - \lambda_{mD}\dfrac{\partial \xi'_{4D0}}{\partial x_D} - f_{s4}\xi'_{4D0} = 0 \\ \left.\dfrac{\partial \xi'_{4D0}}{\partial x_D}\right|_{x_D = x_{eD}} = 0 \\ \xi'_{4D0}|_{x_D=1} = \xi'_{2D0}|_{x_D=1} \end{cases} \tag{A2}$$

The seepage governing equation of region 3 is as follows:

$$\begin{cases} \dfrac{\partial^2 \xi'_{3D0}}{\partial y_D{}^2} + \dfrac{k_{5fi}}{k_{3fi}}\left.\left(\dfrac{\partial \xi'_{5D0}}{\partial x_D} + G\right)\right|_{x_D=1} - f_{s3}\xi'_{3D0} = 0 \\ \left.\dfrac{\partial \xi'_{3D0}}{\partial y_D}\right|_{y_D = y_{eD}} = 0 \\ \xi'_{3D0}|_{y_D=l_d} = \xi'_{2D0}|_{y_D=l_d} \end{cases} \tag{A3}$$

The seepage governing equation of region 2 is as follows:

$$\begin{cases} \dfrac{\partial^2 \xi'_{2D0}}{\partial y_D{}^2} + \dfrac{k_{4fi}}{k_{2fi}}\left.\left(\dfrac{\partial \xi'_{4D0}}{\partial x_D} + G\right)\right|_{x_D=1} - f_{s2}\xi'_{2D0} = 0 \\ \left.\dfrac{\partial \xi'_{2D0}}{\partial y_D}\right|_{y_D = l_D} = \dfrac{1}{M_{32}}\left.\dfrac{\partial \xi'_{3D0}}{\partial y_D}\right|_{y_D = l_D} \\ \xi'_{2D0}|_{y_D=w_D/2} = \xi'_{1D0}|_{y_D=w_D/2} \end{cases} \tag{A4}$$

The seepage governing equation of region 1 is as follows:

$$\begin{cases} \dfrac{\partial^2 \xi'_{1D0}}{\partial x_D{}^2} + \dfrac{2}{C_{FD}}\left.\dfrac{\partial \xi'_{2D0}}{\partial y_D}\right|_{y_D = w_D/2} - \dfrac{s}{\eta_{1D}}\xi'_{1D0} = 0 \\ \left.\dfrac{\partial \xi'_{1D0}}{\partial x_D}\right|_{x_D=0} = -\dfrac{\pi}{C_{FD}} \\ \left.\dfrac{\partial \xi'_{1D0}}{\partial x_D}\right|_{x_D=1} = 0 \end{cases} \tag{A5}$$

First, the governing equations of regions 5 and 4 are solved. Then, the solutions are substituted into the equations of regions 3 and 2, respectively, and the solutions of regions 3 and 2 are obtained in turn. Finally, the solution is substituted into the governing equation of domain 1, and the zeroth-order perturbation solution of region 1 in Laplace space is obtained. The final result is shown in Equation (14).

References

1. Zhang, J.; Qiao, X.R.; Cao, Y.A.; Zhou, J.L.; Shi, D.P. Study and application of lithology identification in igneous hydrocarbon reservoir. *China Foreign Energy* **2006**, *11*, 46–50. [CrossRef]
2. ZHANG, X.D.; Yan, H.U.O.; Bo, B.A.O. The characteristic and distribution rule of the volcanic rock in the northern part of Songliao Basin. *Pet. Geol. Oilfield Dev. Daqing* **2000**, *19*, 10–12. [CrossRef]
3. Cao, B.; Liu, D. Analysis of the distribution, exploration and development characteristics of volcanic oil and gas reservoirs. *Spec. Oil Gas Reserv.* **2004**, *11*, 18–20. [CrossRef]
4. Maxwell, S.C.; Urbancic, T.I.; Steinsberger, N.; Zinno, R. Microseismic Imaging of Hydraulic Fracture Complexity in the Barnett Shale. In Proceedings of the SPE Annual Technical Conference and Exhibition, San Antonio, TX, USA, 29 September–2 October 2002.
5. Fisher, M.K.; Wright, C.A.; Davidson, B.M.; Steinsberger, N.P.; Buckler, W.S.; Goodwin, A.; Fielder, E.O. Integrating Fracture Mapping Technologies to Optimize Stimulations in the Barnett Shale. In Proceedings of the SPE Technical Conference and Exhibition, San Antonio, TX, USA, 29 September–2 October 2002.

6. Fisher, M.K.; Heinze, J.R.; Harris, C.D.; Davidson, B.M.; Wright, C.A.; Dunn, K.P. Optimizing Horizontal Completion Techniques in the Barnett Shale Using Microseismic Fracture Mapping. In Proceedings of the SPE Technical Conference and Exhibition, Houston, TX, USA, 26–29 September 2004.
7. Zhou, W.; Banerjee, R.; Poe, B.; Spath, J.; Thambynayagam, M. Semianalytical Production Simulation of Complex Hydraulic-Fracture Network. *SPE J.* **2014**, *19*, 6–18. [CrossRef]
8. Clarkson, C.R. Production data analysis of unconventional gas wells: Review of theory and best practice. *Int. J. Coal Geol.* **2013**, *109–110*, 101–146. [CrossRef]
9. Lee, S.T.; Brockenbrough, J.R. A New Approximate Analytic Solution for Finite-Conductivity Vertical Fractures. *SPE Form. Eval.* **1986**, *1*, 75–88. [CrossRef]
10. Brown, M.L.; Ozkan, E.; Raghavan, R.; Kazemi, H. Practical Solutions for Pressure-Transient Responses of Fractured Horizontal Wells in Unconventional Shale Reservoirs. *SPE Reserv. Eval. Eng.* **2011**, *14*, 663–676. [CrossRef]
11. Stalgorova, E.; Mattar, L. Practical Analytical Model To Simulate Production of Horizontal Wells With Branch Fractures. In Proceedings of the SPE Canadian Unconventional Resources Conference, Calgary, AB, Canada, 30 October–1 November 2012.
12. Stalgorova, K.; Mattar, L. Analytical Model for Unconventional Multifractured Composite Systems. *SPE Reserv. Eval. Eng.* **2013**, *16*, 246–256. [CrossRef]
13. Yuliang, S.; Wendong, W.; Guanglong, S. Compound flow model of volume fractured horizontal well. *Acta Pet. Sin.* **2014**, *35*, 504–510. [CrossRef]
14. Sureshjani, M.H.; Clarkson, C.R. An Analytical Model for Analyzing and Forecasting Production From Multifractured Horizontal Wells With Complex Branched-Fracture Geometry. *SPE Reserv. Eval. Eng.* **2015**, *18*, 356–374. [CrossRef]
15. Izadi, M.; Haeri, F.; Zeidouni, M. Unconventional multi-fractured analytical solution using dual porosity model. *J. Nat. Gas. Sci. Eng.* **2017**, *45*, 230–242. [CrossRef]
16. Ji, J.; Yao, Y.; Huang, S.; Ma, X.; Zhang, S.; Zhang, F. Analytical model for production performance analysis of multi-fractured horizontal well in tight oil reservoirs. *J. Pet. Sci. Eng.* **2017**, *158*, 380–397. [CrossRef]
17. Jie, G.; Liehui, Z.; Qiguo, L.; Die, Z.; Yulong, Z. Well test model of trilinear flow for fractured horizontal wells in shale gas reservoirs. *Chin. J. Hydrodyn.* **2014**, *29*, 108–113. [CrossRef]
18. Hongjun, Y.; Ermeng, Z.; Jing, F.; Lei, W.; Huiying, Z. Production Analysis of Composite Model of Five Regions for Fractured Horizontal Wells in Shale Gas Reservoirs. *J. Southwest Pet. Univ. (Sci. Technol. Ed.)* **2015**, *3*, 9–16. [CrossRef]
19. Xiaozhe, G.; Changsha, Z. Diffusion Seepage Model for Fractured Horizontal Well in Shale Gas Reservoir. *J. Southwest Pet. Univ. (Sci. Technol. Ed.)* **2015**, *3*, 38–44. [CrossRef]
20. Cossio, M. A Semi-Analytic Solution for Flow in Finite-Conductivity Vertical Fractures Using Fractal Theory. In Proceedings of the SPE Annual Technical Conference and Exhibition, San Antonio, TX, USA, 8–10 October 2004.
21. Sheng, G.; Su, Y.; Wang, W.; Wang, W.J. Well-testing model of fractured horizontal well in fractal reservoir. *J. Liaoning Tech. Univ. (Nat. Sci.)* **2014**, *9*, 1200–1205. [CrossRef]
22. Jing, Z. *Well Testing Analysis for Fractured Well in Stress-Sensitive Formation*; Xi'an Shiyou University: Xi'an, China, 2013.
23. Fuentes-Cruz, G.; Valko, P.P. Revisiting the Dual-Porosity/Dual-Permeability Modeling of Unconventional Reservoirs: The Induced-Interporosity Flow Field. *SPE J.* **2015**, *20*, 124–141. [CrossRef]
24. Jun, Y.; Xiuxing, Y.; Dongyan, F.; Zhixue, S. Trilinear-Flow Well Test Model of Fractured Horizontal Well in Low Permeability Reservoir. *Well Test.* **2011**, *20*, 1–5. [CrossRef]
25. Gang, Z. A Simplified Engineering Model Integrated Stimulated Reservoir Volume (SRV) and Tight Formation Characterization With Multistage Fractured Horizontal Wells. In Proceedings of the SPE Canadian Unconventional Resources Conference, Calgary, AB, Canada, 30 October–1 November 2012.
26. Zhao, Y.L.; Zhang, L.H.; Luo, J.X.; Zhang, B.N. Performance of fractured horizontal well with stimulated reservoir volume in unconventional gas reservoir. *J. Hydrol.* **2014**, *512*, 447–456. [CrossRef]
27. Jiang, R.; Xu, J.; Sun, Z.; Guo, C.; Zhao, Y. Rate Transient Analysis for Multistage Fractured Horizontal Well in Tight Oil Reservoirs considering Stimulated Reservoir Volume. *Math. Probl. Eng.* **2014**, *2014*, 489015. [CrossRef]
28. Sun, L.; Liu, Y.; Wang, Y.; Zhang, Y. Impact of fractured irregular geometry on productivity of multiple fractured horizontal wells in a pressure-sensitive tight oil reservoir. *Pet. Sci. Bull.* **2018**, *1*, 45–56.
29. Sun, R.; Hu, J.; Zhang, Y.; Li, Z. A semi-analytical model for investigating the productivity of fractured horizontal wells in tight oil reservoirs with micro-fractures. *J. Pet. Sci. Eng.* **2020**, *186*, 106781. [CrossRef]
30. Bo, N.; Zuping, X.; Xianshan, L.; Zhijun, L.; Zhonghua, C.; Bocai, J.; Xin, Z.; Huan, T.; Xiaolong, C. Production prediction method of horizontal wells in tight gas reservoirs considering threshold pressure gradient and stress sensitivity. *J. Pet. Sci. Eng.* **2020**, *187*, 106750. [CrossRef]
31. Chen, Z.; Chen, H.; Liao, X.; Zhang, J.; Yu, W. A well-test based study for parameter estimations of artificial fracture networks in the Jimusar shale reservoir in Xinjiang. *Pet. Sci. Bull.* **2019**, *3*, 263–272.
32. Shi, L.; Zhang, K.; Mu, L. Discussion of hydraulic fracturing technical issues in shale oil reservoirs. *Pet. Sci. Bull.* **2020**, *4*, 496–511.
33. Mei, H.; Ma, M.; Yu, Q.; Zhu, F.; Zhang, M. Productivity and influencing factors of the fractured horizontal well in the shale gas reservoir. *Pet. Geol. Oilfield Dev. Daqing* **2019**, *38*, 71–77.
34. Zhang, Q.-S.; He, J.-B.; Hu, Z.-Y.; Yan, Y.-L.; Wang, L. A Production Forecast Model for Multi-fractured Horizontal Well in Low Permeability Reservoirs of Yanchang Oilfield. *Contemp. Chem. Ind.* **2022**, *51*, 1421–1424.

35. Li, Q. Study on Productivity Model of Fractured Horizontal Wells in Volcanic Gas Reservoirs with Natural Fractures. Master's Thesis, The Northeast Petroleum University, Daqing, China, June 2022.
36. Yang, S.L.; Liu, W.Z.; Yu, S.Q.; Wang, G.; Huang, Y. Pore textures and its causes of volcanic reservoir in Songliao Basin. *J. Jilin Univ. (Earth Sci. Ed.)* **2007**, *37*, 506–512. [CrossRef]
37. Yudong, T.; Xiangfang, L.; Baojun, C. Simple analysis on percolation characteristics of volcanic gas reservoir. *Fault-Block Oil Gas Field* **2009**, *16*, 43–45.
38. Barenblatt, G.I.; Zheltov, I.P.; Kochina, I.N. Basic concepts in the theory of seepage of homogeneous liquids in fissured rocks. *J. Appl. Math. Mech.* **1960**, *24*, 1286–1303. [CrossRef]
39. Warren, J.E.; Root, P.J. The Behavior of Naturally Fractured Reservoirs. *SPE J.* **1963**, *3*, 245–255. [CrossRef]
40. De Swaan, O.A. Analytic Solutions for Determining Naturally Fractured Reservoir Properties by Well Testing. *SPE J.* **1976**, *16*, 117–122. [CrossRef]
41. Zhongxiang, C.; Ciqun, L. Theory of Fluid Displacement in a Medium with Double-Porosity. *Acta Mech. Sin.* **1980**, *16*, 4–14. [CrossRef]
42. Xu, J.; Han, G.; Jiang, R.; Deng, Q.; Zhao, Y. Pressure Transient Analysis for Composite Tight Oil Reservoirs after Fracturing. In Proceedings of the SPE North Africa Technical Conference and Exhibition, Cairo, Egypt, 14–16 September 2015.
43. Kikani, J.; Pedrosa, O.A. Perturbation analysis of stress-sensitive reservoirs. *SPE Form. Eval.* **1991**, *6*, 379–386. [CrossRef]
44. Daiyin, Y.; Yazhou, Z.; He, Y.; Chengli, Z. The Numerical Simulation of non-Darcy Flow for YuShulin Low Permeability Oilfield. *Int. J. Control Autom.* **2013**, *6*, 323–344. [CrossRef]
45. Pedrosa, O.A. Pressure Transient Response in Stress-Sensitive Formations. In Proceedings of the SPE California Regional Meeting, Oakland, CA, USA, 2–4 April 1986.
46. Stehfest, H. Algorithm 368: Numerical inversion of Laplace transforms. *Commun. Acm.* **1970**, *13*, 47–49. [CrossRef]
47. Meyer, B.; Bazan, L.; Jacot, R.; Lattibeaudiere, M.G. Optimization of Multiple Transverse Hydraulic Fractures in Horizontal Wellbores. In Proceedings of the SPE Unconventional Gas Conference, Pittsburgh, PA, USA, 23–25 February 2010.